Mechanical Systems and Signal Processing 133 (2019) 106257

Contents lists available at ScienceDirect

Mechanical Systems and Signal Processing

journal homepage: www.elsevier.com/locate/ymssp

Periodic plates with tunneled Acoustic-Black-Holes for directional band gap generation

Liling Tang [a,b], Li Cheng [b,*]

[a] School of Marine Science and Technology, Northwestern Polytechnical University, Xi'an, China
[b] Department of Mechanical Engineering, The Hong Kong Polytechnic University, Hung Hom, Kowloon, Hong Kong, China

ARTICLE INFO

Article history:
Received 22 November 2018
Received in revised form 1 May 2019
Accepted 19 July 2019

Keywords:
Periodic plates
Directional band gaps
Acoustic black hole
Strengthening stud
Vibration attenuation
Flexural waves

ABSTRACT

Research in Acoustic Black Holes (ABHs) attracts increasing interests for its potential applications in vibration control. ABH effect features the energy focalization of flexural waves within a confined area inside a structure with a reducing power-law profiled thickness. With conventional design of ABH structures, however, systematic broadband ABH effects can only be achieved at relatively high frequencies while the mid-to-low frequency application can hardly be envisaged without prohibitively large ABH dimensions. We propose a kind of periodic plates carved inside with tunneled ABHs to achieve directional broad band gaps for flexural waves at mid-to-low frequencies. Analyses on the band structures and mode shapes show the generation of the band gaps through locally resonant effects of the ABH cells. With additional strengthening studs connecting the two ABH branches, Bragg scattering is produced due to its large impedance mismatch with the residual thickness of ABH profile. With the two effects combined, wide band gaps are achieved over a large frequency range for flexural waves travelling along the direction perpendicular to the tunneled ABHs. Both numerical and experimental results show significant attenuation gaps in finite plates with only three ABH cells. The proposed periodic plates with 1D tunneled ABHs and strengthening studs point at potential applications in wave filtering and vibration isolation applications.

1. Introduction

The Acoustic Black Hole (ABH) phenomenon features a reducing local phase velocity of the flexural waves within a power-law profiled structure with a reducing thickness, achieving zero reflection in an ideal scenario with thickness diminishing to zero [1,2]. As a result, compressed waves are stuck in the ABH region with a high energy concentration, conducive to a wide range of applications such as vibration control [3–5], sound radiation reduction [6,7] and energy harvesting [8,9].

Arousing increasing interests in the scientific community, the topic has been widely investigated using single ABH element for both 1D beam [10–12] and 2D plate [5,13–19] structures. Apart from popular numerical methods such as Finite Element or Boundary Elements, various theoretical models have also been developed to study the wave propagation characteristics in structures with single ABH element, exemplified by the geometrical acoustic approach [2], the impedance method [5] and the Rayleigh-Ritz method [10,11,13]. Results show the expected ABH effects in terms of the reduction in the reflection coefficient, energy focalization as well as the potential for vibration control. Experimental investigations have

* Corresponding author.
E-mail address: li.cheng@polyu.edu.hk (L. Cheng).

https://doi.org/10.1016/j.ymssp.2019.106257
0888-3270/

further demonstrated the effectiveness of a single ABH element in damping flexural vibrations [14–17]. However, for a single ABH element, systematic broadband ABH effects can only be achieved above a certain frequency when the incoming wavelength is comparable or smaller than the characteristic dimension of the ABH cell [12,18]. This seriously impedes the application range of the ABH-based technology since the main and the most challenging difficulty is rather in the mid-to-low frequency range. Therefore, extending the ABH effect towards lower frequency region with reasonable structural dimensions is of paramount importance. This dilemma can eventually be resolved by embedding multiple or periodic ABHs into structures. Applying periodic ABHs in beam structures, we demonstrate that broad band gaps can be achieved over a wide frequency range both numerically and experimentally [19,20]. Meanwhile, the proposed structures only require a few ABH elements with small dimensions to achieve considerable broad attenuation bands. This also overcomes the limitations of conventional Phononic Crystals (PCs) based Bragg scattering or locally resonant mechanism [21–25]. The former requires a large number of cells and a large lattice constant to ensure Bragg-type band gaps at mid-to-high frequencies, while the latter can generate resonance-type band gaps at quite low frequencies but with narrow bandwidth. However, the possibility of designing periodic ABHs in 2D plate structures to achieve similar effects remains unknown. It is therefore relevant to investigate whether broad band gaps can also be achieved in plate structures by using periodic ABHs, considering the wider applications of plate structures in practice.

Existing studies on multiple ABHs in plates mainly attempted to apply the ABH effect to achieve vibration [14,16] and sound radiation [6,7] control, with little focus on possible band gaps and wave filtering effect. To the best of our knowledge, based on plane wave expansion method, the only paper dealing with periodic 2D ABHs focuses on the ABH-induced dispersion properties [26], showing no obvious band gaps, possibly due to the complex wave propagation modes/paths in plates. Method-wise, other potential methods, such as the improved fast plane wave expansion [27] and extended plane wave expansion [28] approaches, may be also applied to study periodic structures with ABHs. While understanding that complete band gaps may be difficult to achieve in the general 2D scenario when considering all possible wave modes and paths, we investigate the possibility of generating directional band gaps of flexural propagating waves by proposing a periodic plate with tunneled ABHs. The so-called directional band gaps refer to those frequency bands in which flexural waves are prohibited along a certain propagation direction, specifically x direction in this paper. This study is based on two considerations: on one hand, broad band gaps at mid-to-low frequencies in plate structures certainly deserve more in-depth investigations; on the other hand, considering the complexity of the wave propagations in plates, an effective tuning and manipulations of a certain class of waves along a given direction is of great practical significance for vibration isolation purposes.

In this paper, a plate structure with embedded periodic tunneled ABHs is proposed and modelled by COMSOL Multiphysics in Section 2. The band structures are analyzed in detail in conjunction with typical mode shapes involved. Finite structures with a few ABH elements are compared with their infinite periodic counterparts to understand the observed vibration attenuation bands. In Section 3, strengthening studs are added, aiming at broadening the band gaps over an enlarged frequency range. Then, experimental validations are presented in Section 4 to confirm the numerically predicted phenomena. Finally, conclusions are drawn in Section 5.

2. Periodic plates with tunneled ABHs

As shown in Fig. 1, a unit cell of the proposed periodic plate consists of a plate carved inside with a symmetrical double-leaf 1D ABH profiles forming a tunnel along y-direction. The unit cell has a length, width and thickness of a, b and

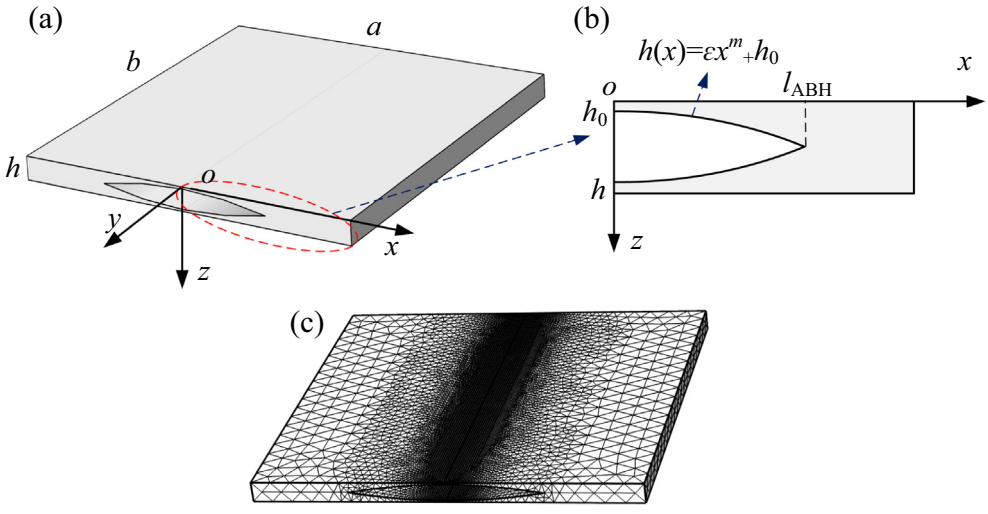

Fig. 1. (a) Unit cell of periodic plates with a uniform plate carved inside by a symmetrical double-leaf ABH tunnel; (b) the cross section of the tunneled ABH whose wall thickness is tapered by $h(x) = \varepsilon x^m + h_0$ with a total pater length of l_{ABH} and a residual thickness of h_0; (c) Mesh of the unit cell.

h, respectively. The cross sectional details of the tunneled ABH are shown in the zoomed in Fig. 1(b). The thickness of each ABH branch is tapered according to $h(x) = \varepsilon x^m + h_0$, where m is a positive rational number, ε is a constant and h_0 is a residual thickness. The total taper length of each ABH branch is l_{ABH}. The unit cells are 1D periodically arranged along the axis x to form either an infinite or finite plate. The double-branch design guarantees structural integrity over the surface and relatively high structural stiffness and strength of the overall structure [29]. To obtain band structures, finite element analyses using COMSOL Multiphysics are conducted to model the unit cell by Solid Mechanics Module. For an infinite plate, the Floquet-Bloch periodic boundary condition is imposed at the edges of the unit cell in x direction and a parametric sweep is applied over the reduced wave vector ka/π. The mesh (as shown in Fig. 1(c)) is physics-controlled with fine element size to ensure a minimum of 6 elements per wavelength for the highest frequency of interest considered here, 8 kHz [30]. In the calculation without specific illustration, a, b and h are set to be 120 mm, 120 mm and 6.4 mm, respectively, with l_{ABH} being 30 mm and h_0 being 0.5 mm. The thickness profile of each ABH branch follows$h(x) = 0.003x^2 + 0.5$ (mm). The material is made of steel with a mass density of 7800 kg/m^3, Young's modulus of 210 GPa, and Poisson's ratio of 0.28.

The calculated band structure is presented in Fig. 2. Several rather flat dispersion curves are observed below 4 kHz as denoted by dark solid lines, which means the near zero group velocity with waves stopping propagating and being confined to a region. This is typical of local resonant characteristics induced by the unique energy focalization feature of the ABH effect, similar to the phenomena observed in beam structures [17,18]. The difference is that these flat dispersion curves are intercepted by a few upward colored curves. Analyses are made to delineate the different natures of the corresponding vibrations. Fig. 3 shows the displacement component distributions of the representative modes T_1, T_2, T_3 and T_4 (also marked in Fig. 2) in x, y, and z directions. The displacement components of mode T_1 show a dominant in-plane vibration in x direction, with an amplitude value much larger than those in the other two directions. These modes represent S0 wave, the dispersion curves of which are marked correspondingly by red dashed lines in Fig. 2. The displacement components of mode T_2 suggest that the vibration in z direction overwhelms that in x direction. The corresponding flexural vibration mainly concentrates on the central part of the ABH cell, exhibiting strong locally resonant characteristics. This can be attributed to the ABH-induced wave speed reduction and energy accumulation effects. Because of the strong coupling between the S0 and the flexural waves induced by the local resonance of the ABH cells, the S0 dispersion curves are split and transit into the flat dispersion curves of flexural waves denoted by red solid lines. Similarly, SH0 dispersion curves, exemplified by the representative T_3 mode with predominant vibration in y direction, are also split and transit into the flat dispersion curves. This is analogous to the well-known veering phenomenon reported in the literatures [31,32]. The transition points are approximately sketched by examining the displacement component distributions to distinguish the wave modes. Therefore, a band gap for all wave modes appears from 3391 Hz to 3698 Hz, as denoted by the blue area in Fig. 2. If only flexural waves are of interest, other types of wave modes can be overlooked. This results in several band gaps as marked by grey areas, which are quite broad at mid-to-low frequencies.

As to the mode T_4 shown in Fig. 3 (j), 3(k), and 3(l), the dominant vibration is in z direction, representing the A0 flexural waves with variations along y direction rather than x direction. As the reduced wave number k approaching 1, representing the limit value for the first irreducible Brillouin zone, the flexural waves propagating at x direction are coupled with those at y direction, marked as yellow solid line. Again, the transition point is approximately sketched. Roughly speaking, when the flexural waves propagating at x direction are coupled in, the dispersion curve trends to be flat. Therefore, directional band gap at x direction exists at very low frequency range, approximately from 370 Hz to 770 Hz in the present case.

Fig. 4 shows the effects of geometrical parameters of the tunneled ABHs, including the power index m and the residual thickness h_0, on the band gaps. It can be seen that considerable band gaps can be achieved and tuned through changing different geometrical parameters. Specifically, increasing m or reducing h_0 would decrease the frequencies of the first band

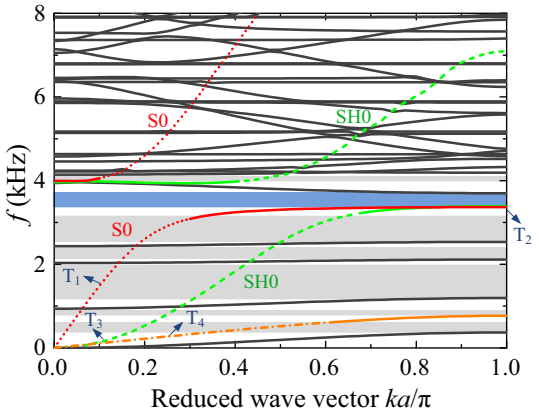

Fig. 2. Band structures in periodic plates with 1D ABH profiles: the blue area denotes band gaps for all wave modes; grey areas denote band gaps only for flexural waves. (For interpretation of the references to colour in this figure legend, the reader is referred to the web version of this article.)

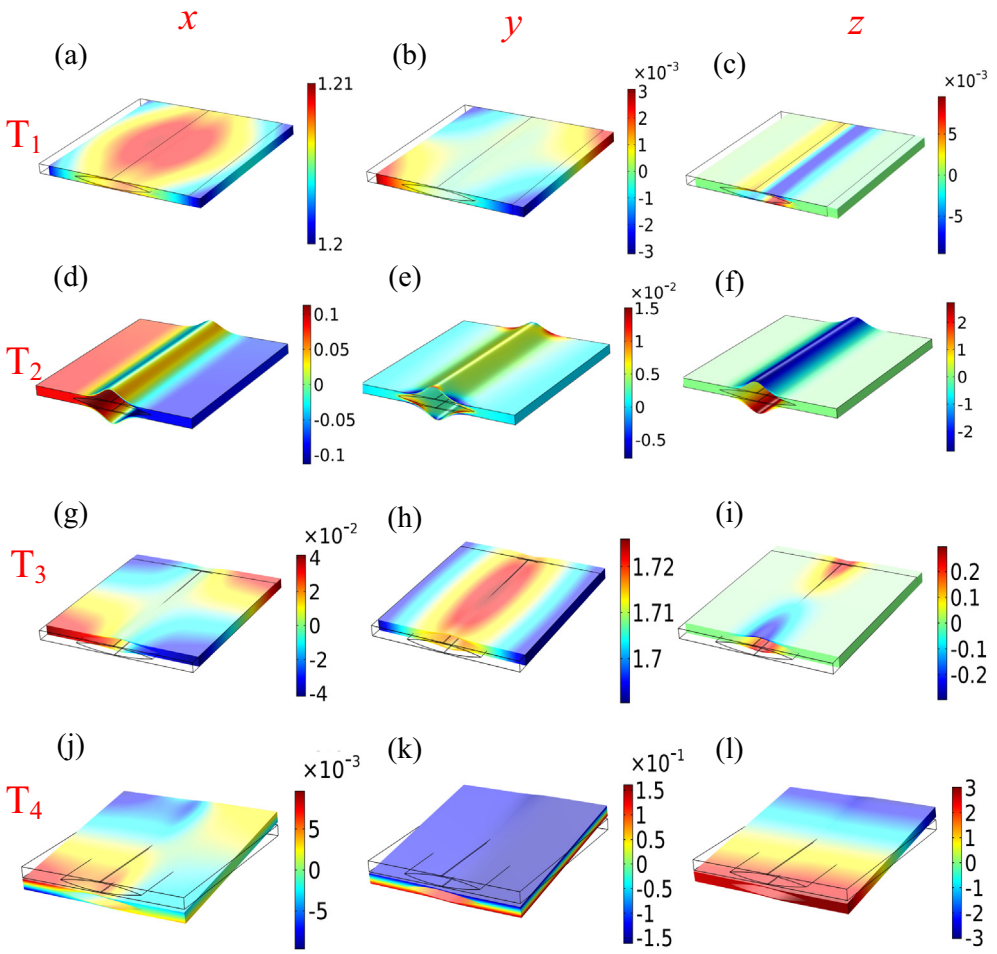

Fig. 3. Displacement component distributions of representative modes T_1, T_2, T_3, T_4 in *x*, *y*, and *z* direction: first row (a), (b), (c) for T_1, representing mode S0; second row (d), (e), (f) for T_2, representing local resonantly flexural mode; third row (g), (h), (i) for T_3, representing mode SH0; Forth row (j), (k), (l) for T4, representing mode A0 propagating in *y* direction.

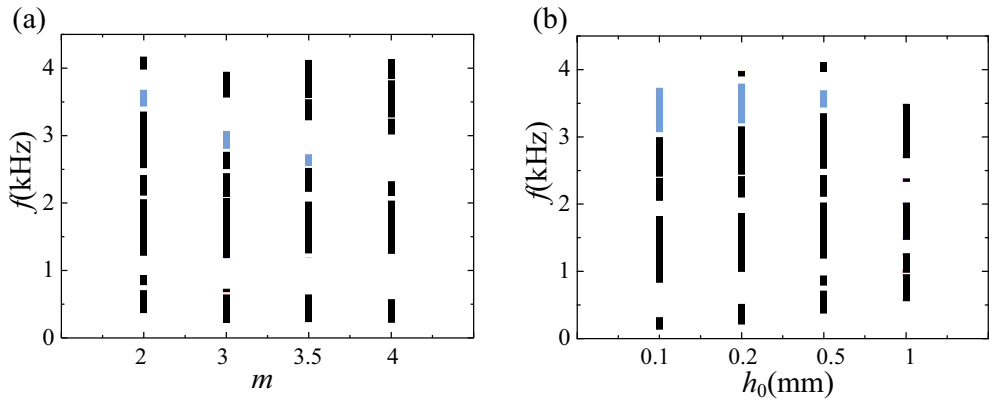

Fig. 4. Effects of (a) the power index *m* and (b) the residual thickness h_0 on the band gaps, where dark lines represent band gaps only for flexural waves while blue lines represent band gaps for all wave modes. (For interpretation of the references to colour in this figure legend, the reader is referred to the web version of this article.)

gap for flexural waves and the band gap for all waves as denoted by blue lines. To be noted, when m is excessively large to violate the smoothness criteria [33] or h_0 is too thick, the band gaps for all waves would no longer exist (see $m = 4$ or $h_0 = 1$ mm). This is because the local resonance is weak resulting from the reduced ABH effect. Overall, we can design reasonable geometrical parameters of the tunneled ABHs to obtain band gaps in targeted frequency bands. In practice, out-of-plane excitations on the plates would mainly generate flexural waves. Therefore, the proposed structures would find their use in the wave filtering design and vibration isolation applications.

To examine the feasibility of achieving the phenomenon in more practical scenarios, finite plates with different number of ABH cells are analyzed to evaluate the vibration attenuation property under free boundary conditions. The damping loss factor of the material is set to be 0.001. A unit harmonic force is applied at one free edge of the plate, 10 mm away from the center along y-direction. Fig. 5 shows the vibration transmissibility, which is defined as $T = 10\log\frac{<V^2>_{\text{out}}}{<V^2>_{\text{in}}}$ with $<V^2>_{\text{in}}$ and $<V^2>_{\text{out}}$ being the mean quadratic velocities at the excitation free end and the other output free end, respectively. A uniform plate with the same dimension as the one when $n = 3$ is included as a reference, showing no noticeable vibration attenuation effect with transmissibility typically oscillating around 0 dB. However, obvious vibration attenuation bands (corresponding to large T values) are visible to cover a large part of the frequency range below 4 kHz for the ABH plates, consistent with the band gaps observed in the infinite periodic plate (marked by shadowed areas). As can be seen, even two ABH cells can achieve considerable attenuation effect. Moreover, an increase in the number of unit cells can create even lower transmissibility to achieve better vibration isolation. The maximum vibration reduction can be up to nearly 70 dB for four ABH cells. It is relevant to note that the extended plane wave expansion (EPWE) can also be used to calculate the attenuation of the unit cell [24,28]. In conclusion, with a few ABH cells, the proposed plate displays high potential in vibration attenuation because of the highly ABH-induced locally resonant effects.

The role of damping layers in achieving ABH effect and in affecting the transmissibility is studied in Fig. 6. The damping layers covering the ABH part of three cells have a thickness of 0.5 mm. The material has a mass density of 950 kg/m^3, Young's modulus of 5 GPa, and Poisson's ratio of 0.3. Uniform plates with and without damping layers are also included as references. As can be seen, for the uniform plate, adding damping layers shows negligible effect on the transmissibility. For the plate with tunneled ABHs, the damping layers do reduce the transmissibility of some resonant peaks because of the local ABH modes. However, systematic ABH attenuation effect by the damping layer cannot be observed because the frequency range is far below the so called cut-on or characteristic frequency of ABHs [12,18], which is 17.4 kHz in the present case. Particularly, damping layers show little effect on the transmissibility within attenuation bands, which confirms that the attenuation bands (corresponding to band gaps in infinite periodic plates) are the inherent characteristic of plates with tunneled ABHs. This is mainly attributed to the local resonance induced by energy focalization of the ABH effect. Therefore, the proposed structures show the superiority in attenuating vibration without applying additional damping layers.

Since energy flux, known as the structural intensity, is useful to visualize the vibration energy propagation, the energy flux and displacement distributions at some typical frequencies in and out of the attenuation bands are also illustrated in Fig. 7. The intensity components in x and y direction can be obtained by $I_i = -\frac{1}{2}\text{Re}\left[\tilde{\sigma}_{ij}\tilde{V}_j^*\right]$ $(i,j = x,y)$, where σ_{ij} is the stress tensor and V_j is the velocity in the j-direction; the superscript $\sim$ and * denote complex number and complex conjugate. As can be seen, at 3180 Hz in the attenuation bands, the displacement field shows that the vibration only concentrates on the first half of the ABH part, close to the excitation. The vibration is significantly reduced after passing through the first ABH cell and becomes barely noticeable in the third ABH cell. The energy flux distribution is exhibited in log scale to reveal the energy flow details with arrows denoting the direction and their corresponding length denoting the magnitude. It confirms that

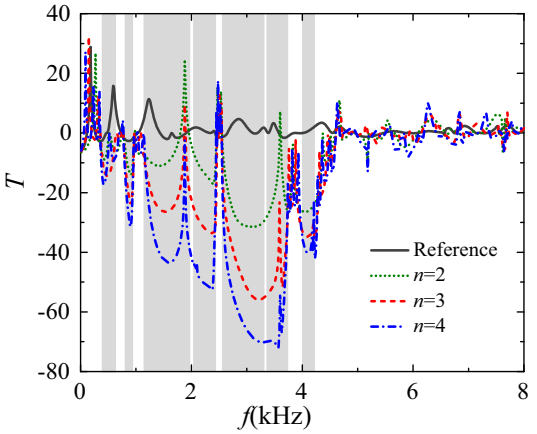

Fig. 5. Transmissibility in finite plates with different number of ABH cells with shadowed areas denoting band gaps in the corresponding infinite periodic plate; a uniform plate with the same dimension as the one when $n = 3$ is also included as a reference.

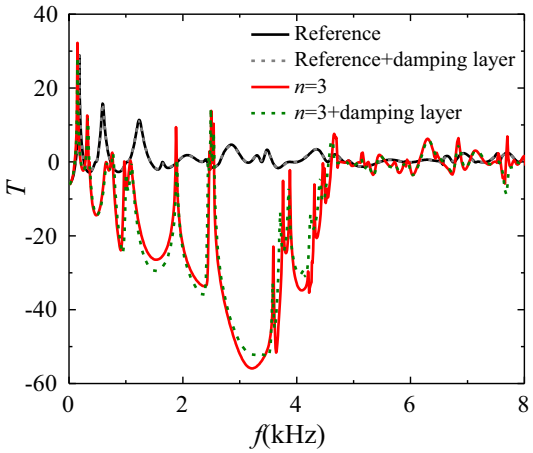

Fig. 6. Transmissibility in a finite plate containing 3 ABH cells with and without damping layers; the uniform cases are included as references.

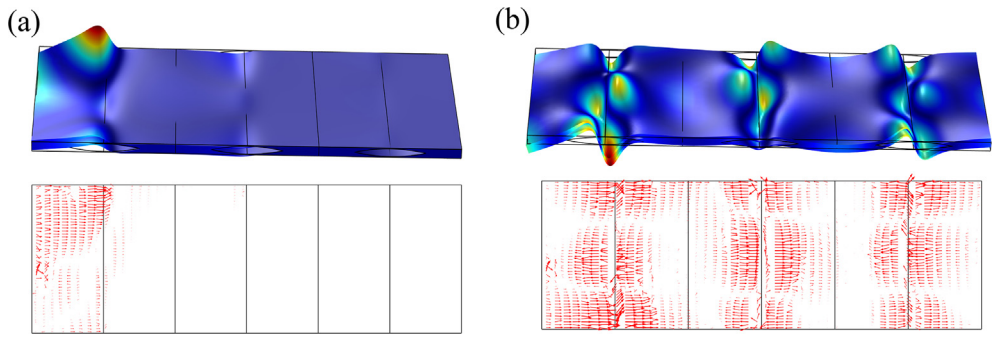

Fig. 7. Displacement and energy flux distributions at typical frequencies in and outside the attenuation bands, respectively: (a) 3180 Hz and (b) 6000 Hz.

the energy is passing from the excitation point to center of the first ABH element. Because of the locally resonant effect, energy is accumulated in the vicinity of the ABH indentation and dissipated by the natural material damping. Therefore, little energy would propagate further or be reflected back, as shown in Fig. 7(a). At 6000 Hz which is outside the attenuation bands, both the displacement and energy flux distributions spread over the three ABH elements and show no wave filtering effect.

3. Periodic plates with strengthening studs

The above periodic plates allow achieving broad band gaps at mid-to-low frequencies. To further enlarge the band gaps to also cover the mid-to-high frequencies, a strengthening stud with a length of Δl is added as shown in Fig. 8. In the numerical calculation, the geometrical and material properties of the plate and the ABH profiles are kept the same as before. The length of the strengthening stud is set to be 10 mm. The calculated band structure is plotted in Fig. 9. It can be seen that in addition to the flat dispersion curves below 4 kHz, flat dispersion curves also appear above 4 kHz. Similar to the case without

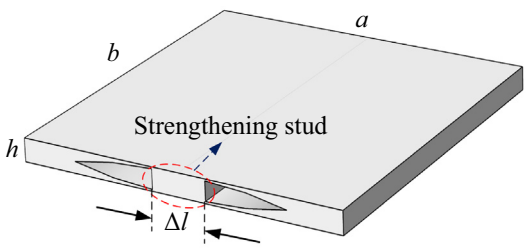

Fig. 8. Unit cell of periodic plates with inside carved by ABH profiles, which are connected by strengthening stud with length ofΔl.

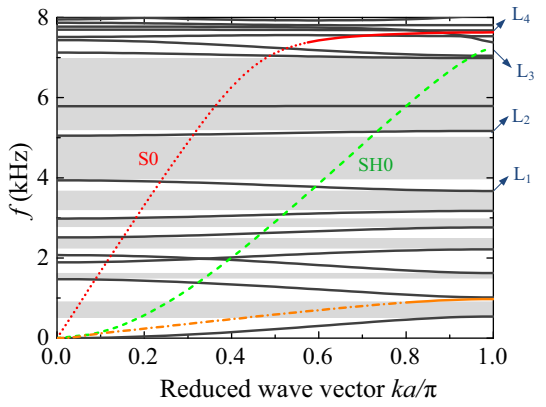

Fig. 9. Band structures in periodic plates with strengthening studs; grey areas denote band gaps for flexural waves.

strengthening studs in Fig. 2, these curves are intercepted by S0 and SH0 as marked by red dashed and green dashed lines. For the same reason stated above, band gaps (marked by grey areas) exist from low to high frequencies within a very large range if only flexural waves are to be taken into consideration. Meanwhile, directional flexural band gaps along *x* direction also exist at very low frequency range since flexural waves marked as dashed yellow line propagate only at *y* direction. These unique properties point at a wider application of the proposed structure in broadband flexural vibration attenuation application.

To clarify the band gap formation mechanism, the total displacement distributions of some selected modes are plotted in Fig. 10. It can be seen that mode L_1 behaves like local resonance of the strengthening stud with ABH branches acting as springs. For modes L_2, L_3 and L_4, however, the ABH parts act as local resonators, which are very similar to the case without strengthening stud. The difference is that the added strengthening stud causes a large impedance mismatch with the thin ABH walls to which it is attached, thus generating the Bragg scattering at mid-to-high frequencies. Meanwhile, owing to the strong energy concentration within the tunneled ABHs, high intensity waves are reflected when reaching the studs. Therefore, the local resonance of ABHs helps to enhance the Bragg scattering effect. With the combined locally resonant and the Bragg scattering effects, these broad band gaps are generated.

Fig. 11 further shows the effect of the length of the strengthening stud on the band gaps. It can be seen that even a very short strengthening stud (Δl=5 mm) would enlarge the band gaps to higher frequencies above 4 kHz because of the induced Bragg scattering effect. Meanwhile, increasing the length of the strengthening length allows enhancing the Bragg scattering effect and therefore enlarging the band gaps at mid-to-high frequencies. This is consistent with the observations made on beam structures [20].

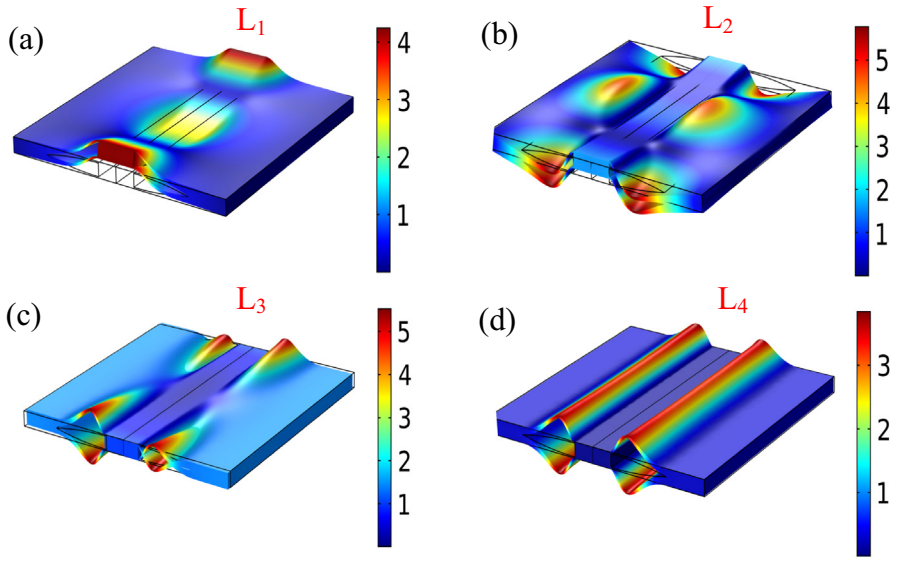

Fig. 10. Total displacement distributions of typical local modes (L_1, L_2, L_3, L_4) marked in Fig. 9.

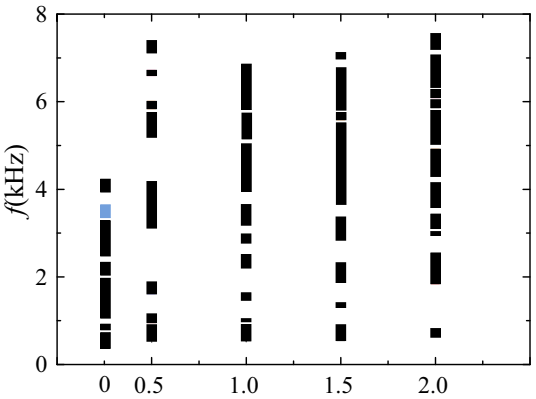

Fig. 11. Effects of length of the strengthening stud Δl on the band gaps, where dark lines represent band gaps only for flexural waves while blue lines represent band gaps for all wave modes. (For interpretation of the references to colour in this figure legend, the reader is referred to the web version of this article.)

Analyses are also conducted on a finite plate with three ABH cells and the strengthening studs under the same boundary and excitation conditions as above. As shown in Fig. 12, the vibration transmissibility curve is plotted and compared with the band gaps, marked by the shadowed areas obtained in the corresponding infinite periodic plate. An untreated uniform plate without obvious attenuation effect is also included as a reference. We can see several attenuation bands both below and above 4 kHz. These attenuation bands are all in good agreement with the band gaps obtained from the infinite periodic plate. It is demonstrated that the proposed plate can be used to efficiently attenuate vibration over a large frequency range by only applying a few cells.

The displacement and energy flux distributions at 6040 Hz in the bottommost of the attenuation bands are also shown in Fig. 13. The concentration of the vibration energy on the first half of ABH element can be clearly observed. Little can be noticed in the subsequent elements as expected, which again confirms the vibration attenuation effect in the proposed plates. Zooming into the details of the energy flux map (bottom sub-figure), we can see that the vibration energy transmits from the excitation point to the thin thickness part of the of the ABH branches, and is then reflected back due to the Bragg scattering from the strengthening stud.

4. Experimental validation

A plate with three ABH elements and strengthening studs was fabricated by 3D printing with steel powder. The material has a mass density of 7765 kg/m^3, Young's modulus of 131 GPa, Poisson's ratio of 0.28, and damping loss factor of 0.001. The length, width and thickness of the plate are 240 mm, 160 mm, and 6 mm, respectively. Each ABH profile follows $h(x) = 0.0003125(x-5)^3 + 0.5$ (mm) with a total length of 20 mm. The length of each strengthening stud is 10 mm. The experiment setup is shown in Fig. 14. The plate was supported by two thin strings to mimic free boundary conditions. Through an electromagnetic shaker amplified by a power amplifier, a periodic chirp signal from 0 to 9 kHz was applied at the

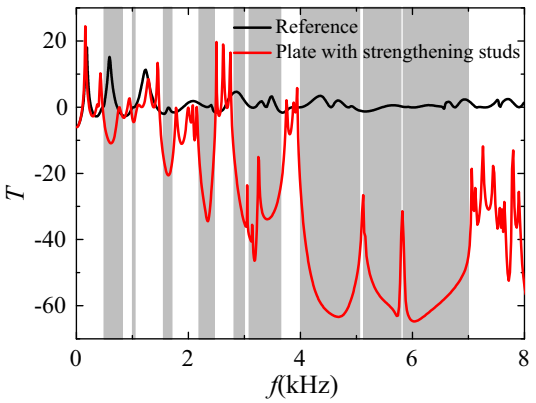

Fig. 12. Vibration transmissibility in a plate containing three tunneled ABHs with strengthening studs; the shadowed areas denote the band gaps corresponding to the infinite periodic plate.

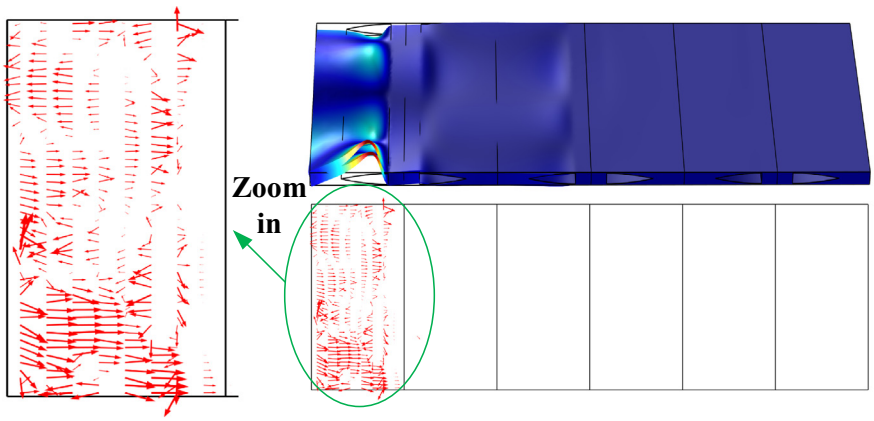

Fig. 13. Displacement and energy flux distributions at selected frequency 6040 Hz.

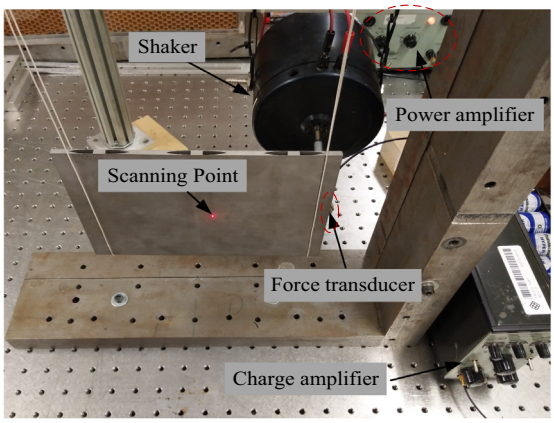

Fig. 14. Experiment setup.

point offset the middle of one free end by 10 mm. The excitation force was measured by a force transducer and amplified by a charge amplifier. A Polytec scanning laser vibrometer was used to measure the vibration response of the plate by scanning 95×47 equally distributed points.

The experimentally measured vibration transmissibility curve is plotted in Fig. 15 and compared with the results from COMSOL simulation. Results agree reasonably well. The differences may be caused by the material property differences

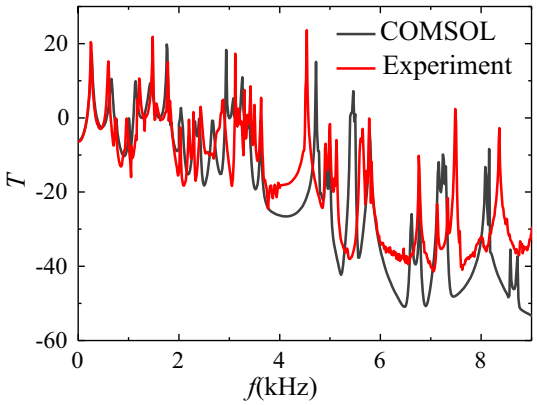

Fig. 15. Vibration transmissibility comparison between the experimental and COMSOL results.

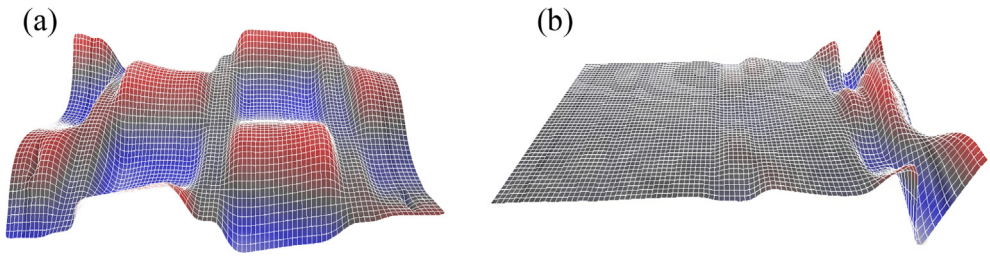

Fig. 16. Displacement shape distributions out and in of the attenuation bands: (a) f = 3430 Hz and (b) f = 7665 Hz.

due to the special processing technology and the torsional modes emerging at higher frequencies, which were not considered in the simulations. Nevertheless, we can see several obvious attenuation bands which indeed cover a large portion of the frequency range considered, especially above 4 kHz. The maximum reduction in experiments is up to 40 dB, albeit a bit lower than the numerically predicted level. One plausible reason is that the vibration level within these attenuation bands is too weak to be accurately measured. Once again, the inevitable excitation of the torsional vibration is also partly responsible. The measured displacement shapes at two selected frequencies, respectively inside and outside the attenuation bands, are given in Fig. 16. It can be seen that beyond the attenuation bands at frequency 3430 Hz, the vibration is more evenly distributed over the entire plate. At 7665 Hz however, in the attenuation gaps, the vibration energy mainly concentrates on the first ABH element, and is significantly reduced after passing through the subsequent ABH elements. Reaching the last element, the remaining vibration becomes unnoticeable. Therefore, we experimentally demonstrate that this kind of plates with only a few ABH elements allows a good flexural wave attenuation.

5. Conclusions

By capitalizing on the ABH-specific features in terms of wave focalization and rich dynamics inside the indentation, we propose a periodic plate with embedded tunneled ABHs. The band structures are studied by using finite element simulations. Results show flat flexural dispersion curves at mid-to-low frequencies due to the ABH-induced locally resonant effects. The S0 and SH0 waves are split as a result of their strong coupling effect with the local flexural waves, leading to the formation of a complete band gap. Meanwhile, several broad band gaps are also achieved at mid-to-low frequencies if only considering the flexural waves. These band gaps would have significantly practical applications in wave filtering and vibration attenuation provided that excitation is mainly out of plane to generate flexural waves. A finite plate with three ABH cells under harmonic excitation is also studied by examining the vibration transmissibility. Considerable attenuation bands are achieved in the mid-to-low frequency range, which is in good agreement with the band gaps obtained from the corresponding infinite periodic plate. The displacement and energy flux distributions in the attenuation bands confirm that the vibration and energy only concentrate on the first ABH part owing to the ABH-specific energy focalization effect.

To enlarge the band gaps towards the mid-to-high frequencies, strengthening studs are added to connect the two branches of tunneled ABHs. The strengthening studs are shown to create a large impedance mismatch with the thin walls of the tunneled ABHs, thus generating effective Bragg scattering. Combined with the locally resonant effect, broad band gaps are obtained within a much broader frequency range. A finite beam with only three ABH cells and strengthening studs confirms the superior vibration attenuation performance of the proposed plate design both numerically and experimentally.

Acknowledgements

This work was supported by the Research Grant Council of the Hong Kong SAR (PolyU 152017/17E), the Fundamental Research Funds for the Central Universities (No. 3102019HHZY03001) and National Science Foundation of China (No. 11532006).

References

[1] M.A. Mironov, Propagation of a flexural wave in a plate whose thickness decreases smoothly to zero in a finite interval, Sov. Phys.: Acoustics 34 (3) (1988) 318–319.
[2] V.V. Krylov, F.J.B.S. Tilman, Acoustic 'black holes' for flexural waves as effective vibration dampers, J. Sound Vib. 274 (2004) 605–619.
[3] D.J. O'Boy, V.V. Krylov, Damping of flexural vibrations in circular plates with tapered central holes, J. Sound Vib. 330 (2011) 2220–2236.
[4] D.J. O'Boy, E.P. Bowyer, V.V. Krylov, Point mobility of a cylindrical plate incorporating a tapered hole of power-law profile, J. Acoust. Soc. Am. 129 (6) (2011) 3475–3482.
[5] V.B. Georgiev, J. Cuenca, F. Gautier, L. Simon, V.V. Krylov, Damping of structural vibrations in beams and elliptical plates using the acoustic black hole effect, J. Sound Vib. 330 (2011) 2497–2508.
[6] S.C. Conlon, J.B. Fahnline, Numerical analysis of the vibroacoustic properties of plates with embedded grids of acoustic black holes, J. Acoust. Soc. Am. 137 (1) (2015) 447–457.
[7] L. Ma, S. Zhang, L. Cheng, A 2D Daubechies wavelet model on the vibration of rectangular plates containing strip indentations with a parabolic thickness profile, J. Sound Vib. 429 (2018) 130–146.

[8] L.X. Zhao, S.C. Conlon, F. Semperlotti, Broadband energy harvesting using acoustic black hole structural tailoring, Smart Mater. Struct. 23 (2014) 065021.
[9] L.X. Zhao, S.C. Conlon, F. Semperlotti, An experimental study of vibration based energy harvesting in dynamically tailored structures with embedded acoustic black holes, Smart Mater. Struct. 24 (2015) 065039.
[10] L.L. Tang, L. Cheng, H. Ji, J. Qiu, Characterization of acoustic black hole effect using a one-dimensional fully-coupled and wavelet-decomposed semi-analytical model, J. Sound Vib. 374 (2016) 172–184.
[11] J. Deng, L. Zheng, P. Zeng, Y. Zuo, O. Guasch, Passive constrained viscoelastic layers to improve the efficiency of truncated acoustic black holes in beams, Mech. Syst. Sig. Process. 118 (2019) 461–476.
[12] L.L. Tang, L. Cheng, Enhanced Acoustic Black Hole effect in beams with a modified thickness profile and extended platform, J. Sound Vib. 391 (2017) 116–126.
[13] D.J. O'Boy, V.V. Krylov, Vibration of a rectangular plate with a central power-law profiled groove by the Rayleigh-Ritz method, Appl. Acoust. 104 (2016) 24–32.
[14] V.V. Krylov, R.E.T.B. Winward, Experimental investigation of the acoustic black hole effect for flexural waves in tapered plates, J. Sound Vib. 300 (1–2) (2007) 43–49.
[15] E.P. Bowyer, V.V. Krylov, Experimental investigation of damping flexural vibrations in glass fibre composite plates containing one- and two-dimensional acoustic black holes, Compos. Struct. 107 (2014) 406–415.
[16] P.A. Feurtado, S. Conlon, An experimental investigation of acoustic black hole dynamics at low, mid, and high frequency, J. Vib. Acoust. 138 (6) (2016) 061002.
[17] H. Ji, J. Luo, J. Qiu, L. Cheng, Investigations on flexural wave propagation and attenuation in a modified one-dimensional acoustic black hole using a laser excitation technique, Mech. Syst. Sig. Process. 104 (2018) 19–35.
[18] S.C. Conlon, J.B. Fahnline, F. Semperlotti, Numuerical analysis of the vibroacoutic properties of plates with embedded grids of acoustic black holes, J. Acoustical Soc. Am. 137 (2015) 447–457.
[19] L.L. Tang, L. Cheng, Broadband local resonant bandgaps in periodic structures with embedded acoustic black holes, J. Appl. Phys. 121 (2017) 194901.
[20] L.L. Tang, L. Cheng, Ultrawide band gaps in phononic beams with double-leaf acoustic black hole indentations, J. Acoustical Soc. Am. 142 (2017) 2802–2807.
[21] A. Martin, M. Kadic, R. Schittny, T. Bückmann, M. Wegener, Phonon band structures of three-dimensional pentamode metamaterials, Phys. Rev. B 86 (2012) 155116.
[22] Y. Xiao, J. Wen, D. Yu, X. Wen, Flexural wave propagation in beams with periodically attached vibration absorbers: Band-gap behavior and band formation mechanisms, J. Sound Vib. 332 (2013) 867.
[23] E.D. Nobrega, F. Gautier, A. Pelat, J.M.C. Dos Santos, Vibration band gaps for elastic metamaterial rods using wave finite element method, Mech. Syst. Sig. Process. 79 (2016) 192–202.
[24] E.J.P. Miranda Jr., E.D. Nobrega, A.H.R. Ferreira, J.M.C. Dos Santos, Flexural wave band gaps in a multi-resonator elastic metamaterial plate using Kirchhoff-Love theory, Mech. Syst. Sig. Process. 116 (2019) 480–504.
[25] C. Sugino, S. Leadenham, M. Ruzzene, A. Ertur, On the mechanism of bandgap formation in locally resonant finite elastic metamaterials, J. Appl. Phys. 120 (2016) 134501.
[26] H. Zhu, F. Semperlotti, Phononic thin plates with embedded acoustic black holes, Phys. Rev. B 91 (10) (2015) 104304.
[27] L. Xie, B. Xia, J. Liu, G. Huang, J. Lei, An improved fast plane wave expansion method for topology optimization of phononic crystals, Int. J. Mech. Sci. 120 (2017) 171–181.
[28] E.J.P. Miranda Jr., J.M.C. Dos Santos, Evanescent Bloch waves and complex band structure in magnetoelectroelastic phononic crystals, Mech. Syst. Sig. Process. 112 (2018) 280–304.
[29] T. Zhou, L.L. Tang, H. Ji, J. Qiu, L. Cheng, Dynamic and static properties of double-layered compound acoustic black hole structures, Int. J. Appl. Mech. 9 (5) (2017) 1750074.
[30] S. Marburg, Discretization requirements: How many elements per wavelength are necessary?, Computational Acoustics of Noise Propagation in Fluids-Finite and Boundary Element Methods, Springer, 2008
[31] A.W. Leissa, On a curve veering aberration, J. Appl. Math. Phys. 25 (1974) 99–111.
[32] E. Manconi, B. Mace, Veering and strong coupling effects in structural dynamics, J. Vib. Acoust. 139 (2017) 021009.
[33] P.A. Feurtado, S.C. Conlon, F. Semperlotti, A normalized wave number variation parameter for acoustic black hole design, J. Acoustical Soc. Am. 136 (2014), EL148-EL152.